PCCP

Theoretical Study of the Electron Tunneling through the Spiral Molecule Junctions along Spiral Paths

Journal:	*Physical Chemistry Chemical Physics*
Manuscript ID	CP-ART-11-2015-006726.R1
Article Type:	Paper
Date Submitted by the Author:	30-Dec-2015

Complete List of Authors:	Xu, Xiaodong; Harbin Institute of Technology, Li, Weiqi; Harbin Institute of Technology, Department of Physics Zhou, Xin; Harbin Institute of Technology, Wang, Qiang; Nanjing Tech University, Department of Applied Chemistry Feng, Ji-kang; Jilin University, Institute of TheoreticalChemistry and College of Chemistry Tian, Wei Quan; Chongqing University, College of Chemistry and Chemical Engineering Jiang, Yongyuan; Harbin Institute of Technology, Department of Physics

Journal Name

ARTICLE

Theoretical Study of the Electron Tunneling through the Spiral Molecule Junctions along Spiral Paths

Xiaodong Xu,[a] Weiqi Li,[a] Xin Zhou,[b] Qiang Wang,[c] Jikang Feng,[d]Weiquan Tian*[e] and Yongyuan Jiang*[a]

Received 00th January 20xx,
Accepted 00th January 20xx

DOI: 10.1039/x0xx00000x

www.rsc.org/

The electronic transport properties of carbohelicenes and heterohelicenes absorbed between two metal electrodes have been investigated by using the nonequilibrium Green's function in combination with the density function theory. The transport property of the molecular junctions is mainly dependent on the nature of spiral molecules. The detailed analyses of the transmission spectrum, the energy levels as well as the spatial distribution of molecular projected self-consistent Hamiltonian explain how the geometry of molecule affects the intra-molecular electronic coupling. The spiral current in the configurations can be achieved by tuning the outer edge states of spiral-shape molecules . Furthermore, the symmetric current-voltage characteristics is investigated with the bias changing for all devices as well as a negative differential resistance behavior.

Introduction

Molecular-scale electronic devices have made a remarkable progress and attracted much attention in recent years[1,2]. Plenty of molecules, especially single-molecule, are expected to be used as the functional building blocks in electronic devices because of their unique properties different from macroscopic systems. Since the concept of individual molecules as active electronic components was proposed[3], molecular electronic devices have been accomplished experimentally and theoretically[4,5]. Numerous amazing characteristics have been proposed and realized, including rectifiers[6-8], negative differential resistances[9], switches[10-12], memories[13] and so on. Although tremendous progress has been made in molecular devices, fundamentals of electronic structure contributions of the building blocks to bulk transport still remains unclear[14-16]. It has been found that many factors can affect the electronic transport properties and rectifying performance, such as the coupling between molecule and electrodes[17], the changing of molecular conformation with applied bias[18], spin-bias-induced charge currents[19,20] etc. In essence, these can be attributed to the structure of molecular wires and the different transmission mechanisms.

Among variety of functional molecules, the helicene is a type of special molecules due to their unique spiral geometry, electronic structure and optical response property[21-24]. Helicenes are polycyclic aromatic compounds with nonplanar spiral-shaped skeletons formed by ortho-fused benzene or other aromatic rings that are endowed with helical chirality. It is the inherently dissymmetric backbone that makes helicenes structurally intriguing for application in the areas of molecular machines, liquid crystal technology and molecular recognition. In addition, their helical topology combined with extended π-conjugated systems can bring strong responses in electronic circular dichroism (ECD). A large number of spiral-shape molecules, such as DNA[25,26], carbohelicenes[27],and heterohelicenes[28-32] and so on, have been discovered and fabricated in biology and chemistry. As a consequence, there has been increasing interest and research activities in this field, and enormous progress has been made in recent decades.

External stimuli, such as light field[33-35], mechanical force[36-38] and magnetic field[39], can be introduced to modulate the molecular conductivity and thus to tune the properties of functional molecular devices. Helicenes, which combine the special optical response[40,41] and quantum transport properties[42,43], might have great potential application in molecular electronics. Under the unequilibrium condition, the junctions might generate spiral current due to molecular spiral geometry which can be used as nano-solenoid-coil to create magnetic field. Though the accurate simulation of magnetic field of helical nano-structures can not be achieved at

[a] *Department of Physics, Harbin Institute of Technology, Harbin, 150001, P. R. China. E-mail: jiangyy@hit.edu.cn*
[b] *Institute of Theoretical and Simulational Chemistry, Academy of Fundamental and Interdisciplinary Sciences, Harbin Institute of Technology, Harbin, 150001, P. R. China.*
[c] *Department of Applied Chemistry, College of Science, Nanjing Tech University, Nanjing, 211816, P. R. China.*
[d] *Institute of Theoretical Chemistry and College of Chemistry Jilin University, 130023, Changchun(P.R.China).*
[e] *College of Chemistry and Chemical Engineering, Chongqing University, Chongqing 400044, P. R. China.*
†Electronic Supplementary Information (ESI) available: [details of any supplementary information available should be included here]. See DOI: 10.1039/x0xx00000x

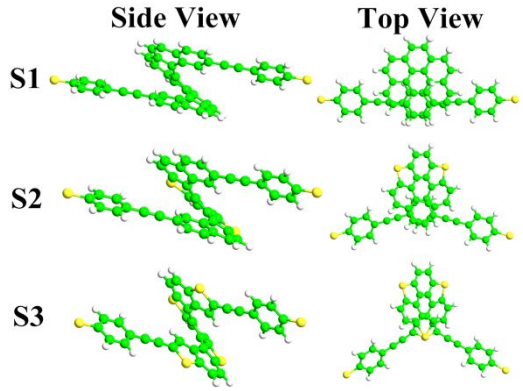

Fig.1 Schematic structures of the spiral-shape molecules, marked as S1, S2 and S3. The left (right) hand of the sketch map represents the side(top) view of the three molecules. The green, yellow and white balls represent carbon, sulfur and hydrogen atoms, respectively. The differences among them are presented at the outer edges of center section while they have the same anchoring groups. At the center section, molecule S1 is made up with the carbon-[7]helicene, while molecule S2 includes five ortho-fused benzenes as well as two thiophenes, and S3 is made up with three ortho-fused benzenes and four thiophenes.

present level of theory, some works show that magnetic field can be produced in molecules or nano-structures external electric field. For example, Barth et al predicted that electron ring currents and induced magnetic fields have been driven in atoms and molecules by circularly polarized laser pulses[44,45]. Recently, Xu et al used tight-binding method(TB) in combination with the non-equilibrium Green's function(NEGF) to predict the magnetic field in some spiral nano-structures[46,47]. However, the studies on the electronic properties of helicenes are rare. In the present work, the electronic transport properties of a certain classical helicenes will be investigated in detail. Incorporating with the properties of the transmission spectrum, the energy levels, the spatial distribution of molecular projected self-consistent Hamiltonian(MPSH) as well as local transmission pathways, the transport mechanism of those helicenes will be revealed in the present work.

Models and calculation methods

To investigate the electronic transport properties of spiral-shape molecules coupling to metal electrodes, three molecules composed by carbohelicenes and two thiol-[7]helicenes with benzenethilates at both sides were designed, which were marked as S1, S2 and S3, respectively(as shown in Fig.1). For single molecular junctions, gold is the most popular to be used as electrodes and thiol group is suitable as anchoring group due to the strong bonding between sulfur atom and gold surface[48-50]. Spiral-shape molecules were coupled with two Au(1 1 1) surfaces, represented by a (5×5) supercell with periodic boundary condition in this work.

The geometry of all spiral molecules were firstly optimized at the B3LYP/6-31G* theoretical level by using the Gaussian 03 software[51], and the optimized molecules are sandwiched between two metal electrodes as shown in Fig.2. All systems were completely optimized until the absolute force on each atom is less than 0.1eV/Å. The electronic transport properties of the molecular junctions were predicted using the NEGF combined with the density functional theory(DFT) method as implemented in ATK software package[52-55] with double-zeta plus polarization basis set for molecules' atoms and single-zeta plus polarization basis set for electrodes' atoms. The GGA-PBE(the generalized gradient approximation with the Perdew-Burke-Ernzerhof parametrization) was utilized as the exchange and correlation functional for all calculations of electron-electron interactions[56]. The mesh energy cutoff of real space for three junctions was tested accurately until the energy changes below 10^{-3}eV and 150Ry was finally chosen to balance the efficiency and the accuracy for electronic transport calculations. The Brillouin zone of all molecular junctions was sampled with 5×5×100 points to improve the calculation accuracy. The current through the molecular junctions was calculated by utilizing the Landauer-Büttiker formula[57,58]:

$$I(V)=\frac{2e}{h}\int T(E,V_b)[f(E-\mu_L)-f(E-\mu_R)]dE$$

where $f(E)$ is the Fermi distribution function, h is Planck's constant, e is electron charge, $\mu_{L(R)}$ is the chemical potential of left(right) electrode where $\mu_L=E_F+eV/2$, $\mu_R=E_F-eV/2$. E_F , the systems' Fermi level,is set to be zero in calculation and $T(E,V_b)$ is the transmission coefficients under different bias obtained by the following formula:

$$T(E,V_b)=T_r[\Gamma_L(E)G^R(E)\Gamma_R(E)G^A(E)]$$

where $G^{R(A)}(E)$ is the retarded or advanced Green's function. $\Gamma_{L(R)}(E)$ is the coupling functions between molecule and electrodes.

Results and Discussion

The equilibrium transport properties of those three molecular junctions under zero bias are shown in Fig.3(a). In the energy region considered for all structures, the first peak of the transmission spectrum under Fermi level, contributed by the

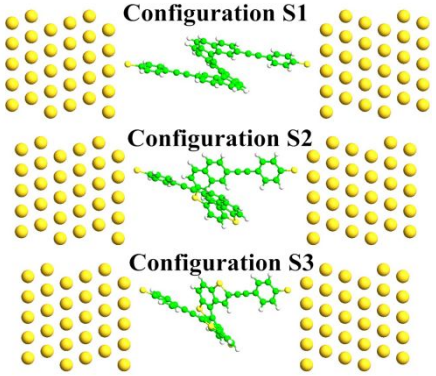

Fig.2 Geometries of the metal-molecule-metal junctions. The spiral-shape molecules are sandwiched between two metallic surfaces of gold. The models of the two-electrode configurations are divided into three regions, including left electrode, scattering region, and right electrode. The sulfur atoms on the both sides of molecules are located at the hollow site on the metallic surfaces.

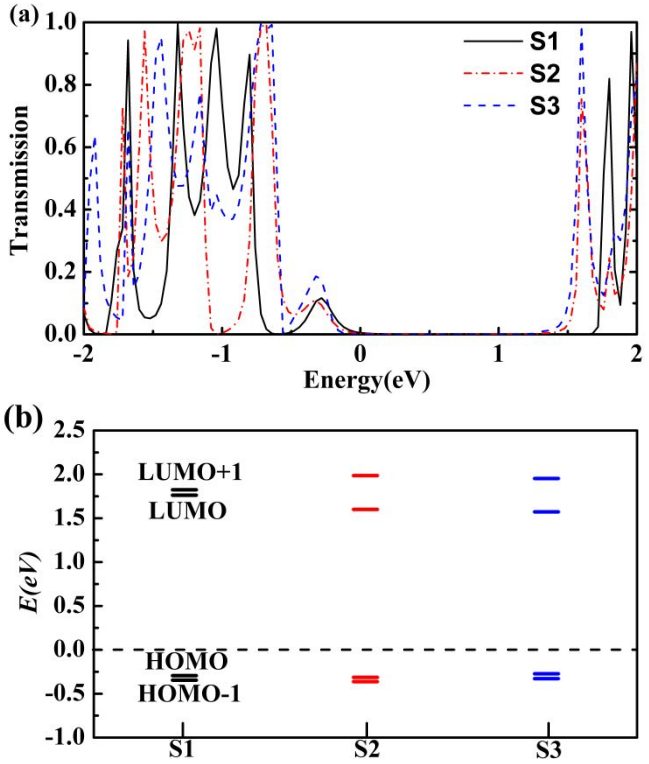

Fig.3 (a)Transmission spectra of the three molecular junctions at zero bias and Fermi level is set to zero. The black solid, red dash dot and blue dash line represents the transmission curve of S1, S2 and S3, respectively. (b) The distribution of the LUMO+1, LUMO, HOMO and HOMO-1 energy levels for three molecules.

highest occupied molecular orbital (HOMO) and the second occupied molecular orbital(HOMO-1) together, plays the major role in electronic transmission while the peak contributed by the lowest unoccupied molecular orbital (LUMO) is far away from Fermi level. The transmission coefficients of structure S3 at the HOMO and HOMO-1 resonance peak under zero bias is larger than that of S1 and S2. Additionally, the transmission spectra also present some differences in position and densities of peak because of the difference of the intra-molecular electronic coupling among the three molecular junctions. Those shifts of transmission peaks can be observed clearly in the molecular orbital energy levels as shown in Fig.3(b). For molecules S1, S2 and S3, the gap between the HOMO and LUMO is 2.05eV, 1.91eV and 1.84eV respectively and the HOMO-1 lies very close to the HOMO displaying remarkable electronic couplings for charge transport. As a result, the significant transmission peak near Fermi level is contributed by the HOMO and HOMO-1 bands together. In addition, the gap between the LUMO and LUMO+1 for structures S2 and S3 is bigger than S1 at zero bias.

To analyze the transport mechanism, the spatial distribution of MPSH is calculated, as exhibited in Fig.4. The position of transmission peak is generally determined by the energy levels of MPSH and the value of transmission peak height is dependent on the delocalization of molecular orbital[41]. The HOMO-1 and HOMO are delocalized over the framework of molecules which provide good channels for electron tunneling through the molecular junctions and lead a significant transmission peak for structures S2 and S3. For S1, the orbital spatial distribution of the HOMO and HOMO-1 is mainly delocalized on the two branches of molecule, which primarily determines the channel of charge tunneling in the interlayer. Besides, the LUMO and LUMO+1 are mainly delocalized at central part of all spiral-shape molecules. Compared the LUMO and LUMO+1 of S3 with the other two molecules, the delocalized electronic density extends to the two terminal sulfur atoms. It indicates that stronger coupling exists between the molecule and electrodes and leads to a higher LUMO transmission peak[59] in correspondence with transmission curves. As mentioned above, due to various properties of the transmission spectra, the energy levels and the electronic structures, unique electronic transport properties are expected for those molecules.

To study the influence of geometry on the electron tunneling through the junctions, the local transmission pathways in molecules have been calculated[60,61]. The local transmission pathways of those three molecular junctions at the HOMO(or HOMO-1) energy level with same threshold at zero bias are shown in Fig.5, respectively. The local transmission is represented by the distribution of arrows on

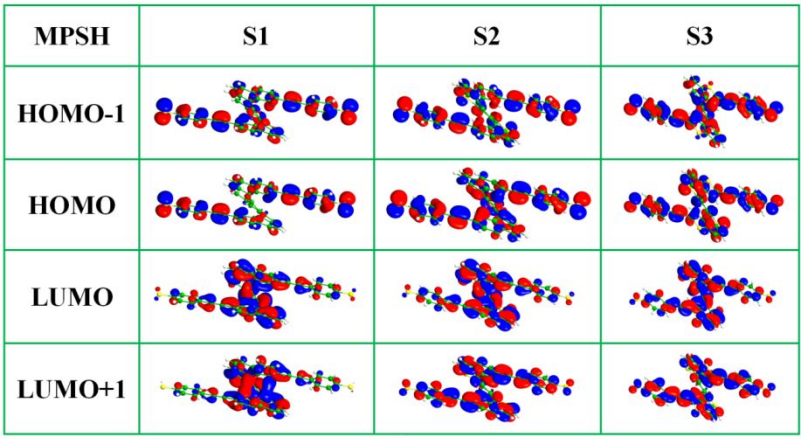

Fig.4 The spatial distributions of the frontier molecular orbital for three molecular junctions at zero bias. The isovalue is set to 0.06 for all plots.

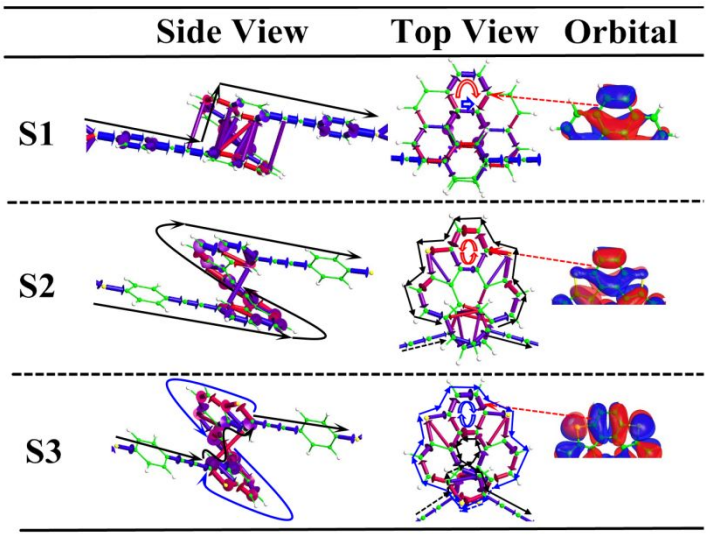

Fig.5 The local transmission pathways through S1, S2 and S3 at energy level of the HOMO under zero bias, respectively. The left (central) part of the sketch map represents the side (top) view of the local transmission. The right part is the molecular orbitals of HOMO distributed on the top hexagon of the top view of those spiral molecules. The lines with arrows indicate the directions of the current.

the molecules and the colors stand for the angle of the transport directions. For molecule S1, there is no spiral current flowing through molecular junction at this energy level,and the total current is offered primarily by tunneling electrons from the top layer to the bottom layer. Obviously, a local loop current (see the top view of S1) which is in the clockwise direction is observed on the top hexagon of S1 molecule, caused by the HOMO distributing on this ring. However, there is an evident spiral current flowing through the molecular junction which appears at the outer edge of molecule S2 along the anticlockwise direction marked in black line. The tunnelling current in the interlayer is also presented while it is only a small contribution for transmission. On the other hand, a local anticlockwise loop current appears on the top hexagon of molecule S2. This is due to a tunneling channel on this ring presented by the HOMO. Importantly, the direction of the loop

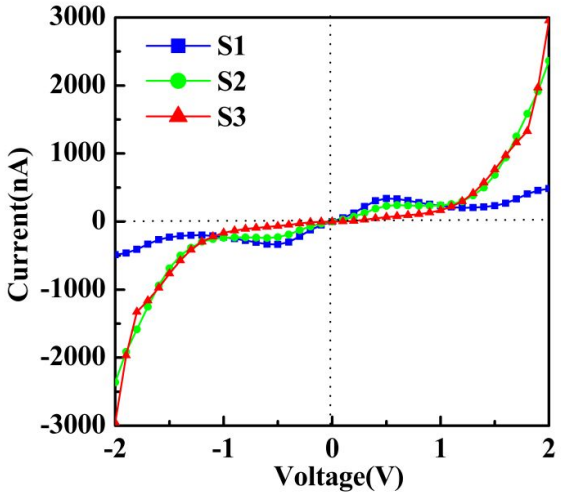

Fig.6 The current-voltage curves of the molecular junctions with bias ranging from -2V to 2V. The blue square line, the green circle line and the red triangle line indicates S1, S2 and S3 molecular junctions.

current depends on the direction of the spiral current at the outer edge. More interestingly, there are two tracks of spiral current presented in molecule S3, but the transport directions are opposite to each other. One of the spiral currents flowing from high potential to low potential transports through the molecule at the inner edge in the anticlockwise direction labelled in black line and the other flowing to high potential transports through the molecule at the outer edge in the clockwise direction labelled in blue line. Similarly, the molecule S3 has a local loop current which is in clockwise direction and tunnelling current in the interlayer. We can draw a semblable consequence that the loop current is caused by the HOMO localized on the top hexagon of those molecules and its direction is determined by the direction of spiral current at edges. Not only spiral current but also local loop current can be expected to generate magnetic field. One of the reasons for the different transmission pathways is the distance between the top and the bottom aromatic rings of spiral molecules, and the distance of the nearest atoms between layers for S1, S2 and S3 is 3.0Å, 3.14Å, 3.21Å respectively. Namely, small interlayer distance increases the chance of interlayer electron tunneling. Moreover, directed electron circulation may produce an induced magnetic field，which makes these structures suitable for special application in molecular devices, for example, nano-solenoid-coil.

From the features of the current through the molecular junctions at the nonequilibrium condition, more about the transport property of the three structures can be revealed. Fig.6 exhibits the current-voltage(I-V) curves of the molecular junctions with bias ranging from -2.0V to 2.0V. Under positive or negative bias, the current-voltage curves have a same trend of variation for every molecules, and the transport properties of the devices are strongly dependent on the variety of molecules. For example, as shown in Fig.6, when the bias voltage increases from 0V to 0.5V, the current will increase gradually for all structures. However, with the voltage increasing from 0.5V to 1.1V, the current in S1 and S2 decreases slightly while the current of S3 still remains

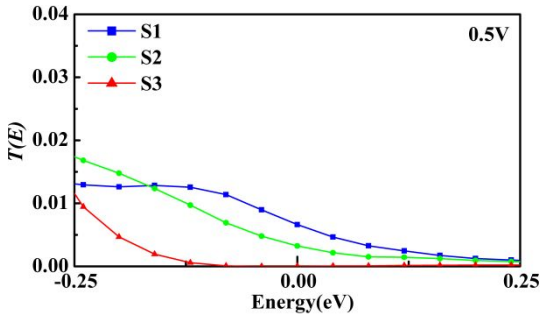

Fig.7 The portion of transmission spectrum locating in the bias window at 0.5V voltage. The bias window ranges from -0.25eV to 0.25eV, and the blue square, the green circle and the red triangle line indicates S1, S2 and S3, respectively.

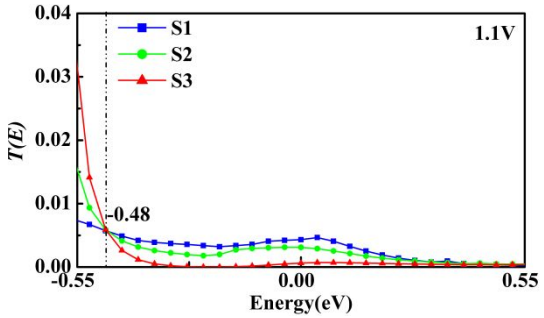

Fig.8 The portion of transmission spectrum locating in the bias window at 1.1V voltage. The bias window ranges from -0.55eV to 0.55eV, and the blue square, the green circle line and the red triangle line indicates S1, S2 and S3, respectively.

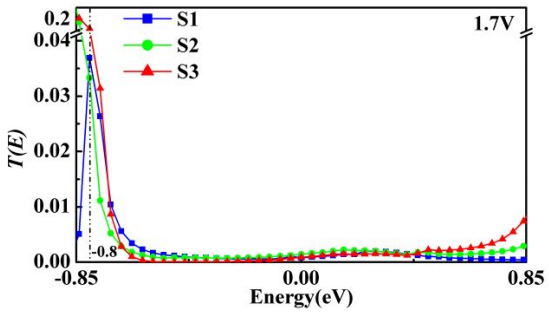

Fig.9 The portion of transmission spectrum locating in the bias window at 1.7V voltage. The bias window ranges from -0.85eV to 0.85eV , and the blue square, the green circle and the red triangle line indicates S1, S2 and S3, respectively.

increasing. The current value with the bias voltage ranging from 0V to 1.1V follows the order of S1>S2>S3, in line with the transmission spectra. The reasons for these behaviors are all rooted in the transmission peak of S1 near Fermi level has a bigger section entering bias window, which primarily makes contribution to current integral. More interestingly, the three current-voltage curves have an intersection near bias voltage 1.1V. With the bias further increasing , the current in S2 and S3 has a rapid increase while S1 still keeps dropping until the bias voltage exceeds 1.4V. To describe the current trend in detail, applied bias at 0.5V, 1.1V and 1.7V were chosen to analyze, respectively. It is well known that the current is determined by the integral of the portion of transmission entering bias window. Under 0.5V bias, the bias window ranges from -0.25eV to 0.25eV, the portion of transmission spectrum entering bias window is presented in Fig.7. It is obvious to observe that the relationship of transmission spectrum in this bias window is T(S1)>T(S2)>T(S3) which leads a current value order of I(S1)>I(S2)>I(S3). Fig.8 shows the transmission spectra with bias window ranging -0.55eV to 0.55eV under 1.1V bias and the order of transmission spectra of those molecular junctions is T(S1)>T(S2)>T(S3) in [-0.55eV,-0.48eV] energy region while the order gets reversed in [-0.48eV,0.55eV] energy region. The integral of transmission spectra of those molecular junctions finally leads to a similar value of current. In Fig.9, transmission spectrum of S1 is much lower than S2 and S3 in [-0.85eV,-0.8eV] energy region which determines the order of the transmission spectra approximating to T(S3)≈T(S2)>>T(S1) and the integral of transmission spectra finally gets a current order of I(S3)≈I(S2)>I(S1) at 1.7V bias. According to analyses above, the transport properties of those molecular junctions can be understood deeply.

Another interesting phenomenon shown in I-V curves is the negative differential resistance behavior(called NDR as well) in configuration S1 and S2. To understand NDR of those molecular junctions clearly, the transmission spectra and the corresponding PDOS(projected density of states) at 0.5V, 0.8V, 1.1V bias is analyzed in detail, as presented in Fig.10. Due to the PDOS gives information of the molecular orbital contributing to the eigenstate of the junctions and the transmission reveals a clear correspondence to the PDOS, the

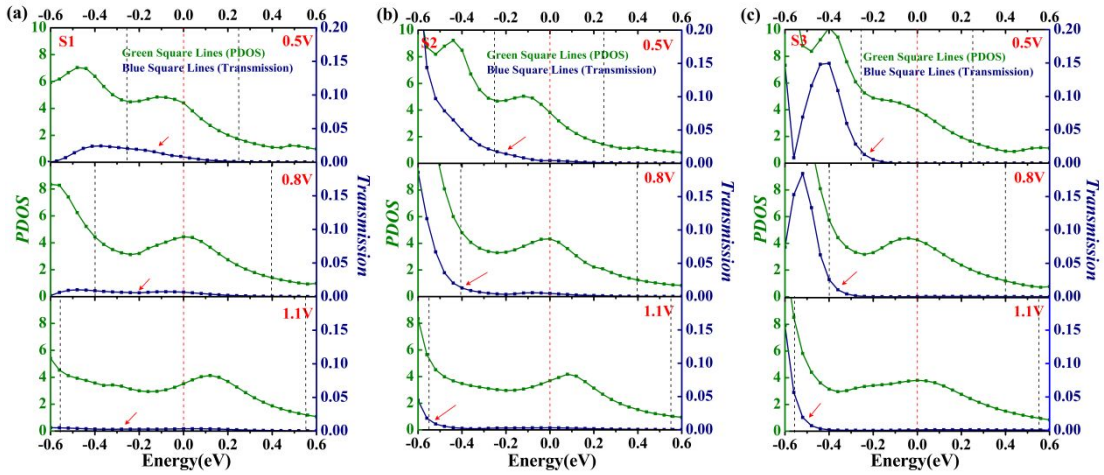

Fig.10 The changes of transmission spectrum and corresponding PDOS of molecular junctions S1, S2 and S3 under the bias voltages of 0.5V, 0.8, 1.1V. The green and blue square lines represent the corresponding PDOS and the transmission spectrum , accordingly. The black dash lines indicate the bias window and red dash lines is Fermi level.

mechanism of the NDR can be expounded by the evolution of the PDOS and transmission spectra in bias windows. For S1(Fig10(a)), obviously, there is a big part of transmission spectrum entering bias window at 0.5V bias. As the bias increases from 0.5V to 0.8V, the portion of transmission spectrum in bias window have a decrease caused by the PDOS. As a result, a decrease appears in current. When bias increases further, the strength of transmission spectrum in bias window becomes weaker leading a decrease in current as well. Namely, an NDR behavior occurs in molecular junction S1. Similarly, there is a decrease in current with bias increasing from 0.5V to 1.1V consistent with the evolution of transmission spectrum and PDOS, as shown in Fig10(b). It indicates that an NDR behavior also appears in the molecular junction S2. Interestingly, a sharp contrast to S1 and S2 is that there is no NDR behavior observed in the current-voltage correlation of molecular junction S3, presented by the the sustainable growth of the transmission spectra and PDOS in the bias windows from 0.5V to 1.1V, as shown in Fig10(c).

Further investigation have been conducted about the influence of the self-interaction on the electronic transport properties of those spiral molecules. The disagreement of the transport properties of molecular junctions between theory and experiment remains large, even for simple molecules, some other influence factors should be been taken into account, such as electrodes[62], the position of molecules[63], anchoring groups[64] and the self-interaction of molecules[65] and so on. Many investigations have confirmed that the theoretical predictions are in much closer agreement with experiments when self-interaction corrected exchange and correlation functionals are employed[66,67]. The GGA+U approach was employed to investigate the influence of the self-interaction on the molecular junction S2. As a result, the transport properties are primarily effected by the self-interaction. The modulation of current can be predicted by transmission spectra with different corrections of U (see supplementary information). Additionally, the spiral current at the outer edges of molecule S2 always exists and some other tunneling channels are opened with the value of U increasing(shown in Fig.S1). As the systematic error of the method exists in all predictions of those systems, thus the variation pattern of electro-magnetic properties would be similar if self-interaction correction is taken into account.

Conclusions

In summary, the electronic transport properties of spiral-shape molecules sandwiched between gold electrodes have been studied by the first principles calculations. The spiral-shape molecules have similar spiral geometry but different components leading to their unique electronic properties. There is no spiral current flowing through molecule S1 and the total current is only offered by electron tunneling in the interlayer. When the thiophene rings are introduced in helicenes like molecule S2 and S3, molecular conformations and electron distribution of frontier orbitals will vary, then the spiral current appears, which provides the possibility to generate magnetic field. The local loop current observed in the molecules S2 and S3 is caused by the molecule orbital distribution, and its direction is primarily depended on the direction of the spiral current at the edges. Additionally, the current-voltage curves indicate that an NDR behavior occurs in structures S1 and S2 but does not present in S3. In low bias, the order of current value among three structures is S1>S2>S3. With the bias increasing further, the order will shift to S1<<S2 $\approx$ S3, meaning that the shift of the current-voltage curves presents a switching effect. The present work provides useful information for the application of spiral-shape molecules in the field of molecule solenoid and other functional components.

Acknowledgements

This work is supported by Natural Science Foundation of China under grant numbers (11104048, 21303030, 21203094, and 21373112), the State Key Lab of Urban Water Resource and Environment (HIT) (2014TS01), and the Open Project of State Key Laboratory of Supramolecular Structure and Materials (JLU) (SKLSSM2015018).

References

1 A. Nitzan and M. A. Ratner, *Science*, 2003, **300**, 1384-1389.
2 C. Huang, A. V. Rudnev, W. Hong and T. Wandlowski, *Chemical Society Reviews*, 2015, **44**, 889-901.
3 A. Aviram and M. A. Ratner, *Chemical Physics Letters*, 1974, **29**, 277-283.
4 M. Paulsson, T. Frederiksen and M. Brandbyge, *Nano Letters*, 2006, **6**, 258-262.
5 H. Rascón-Ramos, J. M. Artés, Y. Li and J. Hihath, *Nature Materials*, 2015, **14**, 517-522.
6 A. Martin, J. Sambles and G. Ashwell, *Physical Review Letters*, 1993, **70**, 218.
7 J. Taylor, M. Brandbyge and K. Stokbro, *Physical Review Letters*, 2002, **89**, 138301.
8 H. Liu, Y. He, J. Zhang, J. Zhao and L. Chen, *Physical Chemistry Chemical Physics*, 2015, **17**, 4558-4568.
9 J. Chen, M. Reed, A. Rawlett and J. Tour, *Science*, 1999, **286**, 1550-1552.
10 J. L. Zhang, J. Q. Zhong, J. D. Lin, W. P. Hu, K. Wu, G. Q. Xu, A. T. Wee and W. Chen, *Chemical Society Reviews*, 2015, **44**, 2998-3022.
11 J. Taylor, M. Brandbyge and K. Stokbro, *Physical Review B*, 2003, **68**, 121101.
12 J. Zhao, W. Zhao, B. Cui, C. Fang, Y. Xu, X. Kong, D. Li and D. Liu, *RSC Advances*, 2014, **4**, 40941-40950.
13 M. Reed, J. Chen, A. Rawlett, D. Price and J. Tour, *Applied Physics Letters*, 2001, **78**, 3735-3737.
14 M. Di Ventra, S. Pantelides and N. Lang, *Physical Review Letters*, 2000, **84**, 979.
15 S. M. Lindsay and M. A. Ratner, *Advanced Materials*, 2007, 19, 23-31.
16 M. A. Reed, C. Zhou, C. Muller, T. Burgin and J. Tour, *Science*, 1997, **278**, 252-254.
17 V. V. Zhirnov and R. K. Cavin, *Nature Materials*, 2006, **5**, 11-12.
18 W. Haiss, C. Wang, I. Grace, A. S. Batsanov, D. J. Schiffrin, S. J. Higgins, M. R. Bryce, C. J. Lambert and R. J. Nichols, *Nature Materials*, 2006, **5**, 995-1002.
19 F. Zhai, X. Zhao and H. Xu, *Applied Physics Letters*, 2009, **94**, 262103.
20 Q. Wu, P. Zhao, Y. Su, S. Li, J. Guo and G. Chen, *RSC Advances*, 2015, **5**, 52938-52944.
21 A. Bossi, E. Licandro, S. Maiorana, C. Rigamonti, S. Righetto, G. R. Stephenson, M. Spassova, E. Botek and B. Champagne, *The Journal of Physical Chemistry C*, 2008, **112**, 7900-7907.

22 B. Jansík, A. Rizzo, H. Ågren and B. Champagne, *Journal of Chemical Theory and Computation*, 2008,**4**,457-467.
23 A. Rajca, M. Pink, S. Xiao, M. Miyasaka, S. Rajca, K. Das and K. Plessel, *The Journal of Organic Chemistry*, 2009, **74**, 7504-7513.
24 J. Heurich, J. Cuevas, W. Wenzel and G. Schön, *Physical Review Letters*, 2002, **88**, 256803.
25 D. Klotsa, R. A. Römer and M. S. Turner, *Biophysical Journal*, 2005, **89**, 2187-2198.
26 C. Dekker and M. A. Ratner, *Phys. World*, 2001, **14**, 29-33.
27 R. Martin and M. Baes, *Tetrahedron*, 1975, **31**, 2135-2137.
28 H. Oyama, K. Nakano, T. Harada, R. Kuroda, M. Naito, K. Nobusawa and K. Nozaki, *Organic Letters*, 2013, **15**, 2104-2107.
29 K. Nakano, H. Oyama, Y. Nishimura, S. Nakasako and K. Nozaki, *Angewandte Chemie*, 2012, **124**, 719-723.
30 P. Sehnal, I. G. Stará, D. Šaman, M. Tichý, J. Míšek, J. Cvačka, L. Rulíšek, J. Chocholoušová, J. Vacek and G. Goryl, *Proceedings of the National Academy of Sciences*, 2009, **106**, 13169-13174.
31 M. Miyasaka, A. Rajca, M. Pink and S. Rajca, *Journal of the American Chemical Society*, 2005, **127**, 13806-13807.
32 C. E. Szakacs and P. G. Mezey, The Journal of Physical Chemistry A, 2008, **112**, 6783-6787.
33 W. R. Browne and B. L. Feringa, *Annual Review of PhysicalChemistry*, 2009, **60**, 407-428.
34 I. L. Fabelinskii, Molecular scattering of light, *Springer Science & Business Media*, 2012.
35 K. Takahashi, H.-B. Cui, Y. Okano, H. Kobayashi, Y. Einaga and O. Sato, *Inorganic Chemistry*, 2006, **45**, 5739-5741.
36 X. Cui, A. Primak, X. Zarate, J. Tomfohr, O. Sankey, A. Moore, T. Moore, D. Gust, G. Harris and S. Lindsay, *Science*, 2001, **294**, 571-574.
37 B. I. Yakobson and R. E. Smalley, *American Scientist*, 1997, 324-337.
38 K. C. Neuman and A. Nagy, *Nature Methods*, 2008, **5**, 491-505.
39 F. Schedin, A. Geim, S. Morozov, E. Hill, P. Blake, M. Katsnelson and K. Novoselov, *Nature Materials*, 2007, **6**, 652-655.
40 E. Botek, J.-M. André, B. Champagne, T. Verbiest and A. Persoons, *The Journal of Chemical Physics*, 2005, **122**, 234713.
41 E. Botek, B. Champagne, M. Turki and J.-M. André, *The Journal of Chemical Physics*, 2004, **120**, 2042-2048.
42 G. L. Zhang, H. L. Yuan, H. Zhang, Y. Shang and M. Sun, *International Journal of Quantum Chemistry*, 2011, **111**, 4214-4223.
43 G. Zhang, D. Li, Y. Shang, H. Zhang, M. Sun, B. Liu and Z. Li, *The Journal of Physical Chemistry C*, 2011, **115**, 5257-5264.
44 I. Barth and J. Manz, *Physical Review A*, 2007, **75**, 012510.
45 I. Barth, L. Serrano-Andrés and T. Seideman, *The Journal of Chemical Physics*, 2008, **129**, 164303.
46 F. Xu, A. Sadrzadeh, Z. Xu and B. I. Yakobson, *Computational Materials Science*, 2014, **83**, 426-433.
47 F. Xu, H. Yu, A. Sadrzadeh and B. I. Yakobson, *Nano Letters*, 2015.
48 W. Andreoni, A. Curioni and H. Grönbeck, *International Journal of Quantum Chemistry*, 2000, **80**, 598-608.
49 M. Ford, R. Hoft and J. Gale, *Molecular Simulation*, 2006, **32**, 1219-1225.
50 F. Tielens and E. Santos, *The Journal of Physical Chemistry C*, 2010, **114**, 9444-9452.
51 M.J. Frisch, G.W. Trucks, H.B. Schlegel, G.E. Scuseria, M.A. Robb, J.R. Cheeseman, J.A. Montgomery, Jr., T. Vreven, K.N. Kudin, J.C. Burant, J.M. Millam, S.S. Iyengar, J. Tomasi, V. Barone, B. Mennucci, M. Cossi, G. Scalmani, N. Rega, G.A. Petersson, H. Nakatsuji, M. Hada, M. Ehara, K. Toyota, R. Ukuda, J. Hasegawa, M. Ishida, T. Nakajima, Y. Honda, O. Kitao, H. Nakai, M. Klene, X. Li, J.E. Knox, H.P. Hratchian, J.B. Cross, C. Adamo, J. Jaramillo, R. Gomperts, R.E. Stratmann, O., Yazyev, A.J. Austin, R. Cammi, C. Pomelli, J.W. Ochterski, P.Y. Ayala, K. Morokuma, G.A. Voth, P. Salvador, J.J. Dannenberg, V.G. Zakrzewski, S. Dapprich, A.D. Daniels, M. C. Strain, O. Farkas, D.K. Malick, A.D. Rabuck, K. Raghavachari, J.B. Foresman, J.V. Ortiz, Q. Cui, A.G. Baboul, S. Clifford, J. Cioslowski, B.B. Stefanov, G. Liu, A. Liashenko, P. Piskorz, I. Komaromi, R.L. Martin, D.J. Fox, T. Keith, M.A. Al-Laham, C.Y. Peng, A. Anayakkara, M. Challacombe, P.M.W. Gill, B. Johnson, W. Chen, M.W. Wong, C. Gonzalez, J.A. Pople, 2003. Gaussian 03, Revision B.05, Pople, Gaussian Inc., Pittsburgh, PA, 2003.
52 M. Brandbyge, J.-L. Mozos, P. Ordejón, J. Taylor and K. Stokbro, *Physical Review B*, 2002, **65**, 165401.
53 J. Taylor, H. Guo and J. Wang, *Physical Review B*, 2001, **63**, 121104.
54 Atomistix Toolkit, QuantumWise A/S, (**www.quantumwise.com**)
55 J. Taylor, H. Guo and J. Wang, *Physical Review B*, 2001, **63**, 245407.
56 J. P. Perdew, K. Burke and M. Ernzerhof, *Physical Review Letters*, 1996, **77**, 3865.
57 Y. Meir and N. S. Wingreen, *Physical Review Letters*, 1992, **68**, 2512.
58 M. Büttiker, Y. Imry, R. Landauer and S. Pinhas, *Physical Review B*, 1985, **31**, 6207.
59 M. Kiguchi and S. Kaneko, *Physical Chemistry Chemical Physics*, 2013, **15**, 2253-2267.
60 G. C. Solomon, C. Herrmann, T. Hansen, V. Mujica and M. A. Ratner, *Nature Chemistry*, 2010, **2**, 223-228.
61 G. C. Solomon, C. Herrmann, J. Vura-Weis, M. R. Wasielewski and M. A. Ratner, *Journal of the American Chemical Society*, 2010, **132**, 7887-7889.
62 R. Matsushita and M. Kiguchi, *Physical Chemistry Chemical Physics*, 2015, **17**, 21254-21260.
63 H. Liu, Y. He, J. Zhang, J. Zhao and L. Chen, *Physical Chemistry Chemical Physics*, 2015, **17**, 4558-4568.
64 V. Kaliginedi, A. V. Rudnev, P. Moreno-García, M. Baghernejad, C. Huang, W. Hong and T. Wandlowski, *Physical Chemistry Chemical Physics*, 2014, **16**, 23529-23539.
65 C. Toher, A. Filippetti, S. Sanvito and K. Burke, *Physical Review Letters*, 2005, **95**, 146402.
66 R. B. Pontes, A. R. Rocha, S. Sanvito, A. Fazzio and A. o. J. R. da Silva, *ACS Nano*, 2011, 5, 795-804.
67 A. de Melo Souza, I. Rungger, R. B. Pontes, A. R. Rocha, A. J. R. da Silva, U. Schwingenschlöegl and S. Sanvito, *Nanoscale*, 2014, **6**, 14495-14507.